The 9th European Congress on Computational Methods in Applied Sciences and Engineering
ECCOMAS Congress 2024
3–7 June 2024, Lisboa, Portugal

CONSISTENT DISCRETIZATION SCHEMES FOR THE CONTINUOUS ADJOINT EQUATIONS IN AERODYNAMIC SHAPE OPTIMIZATION FOR TURBULENT/TRANSITIONAL FLOWS

MARINA G. KONTOU, XENOFON S. TROMPOUKIS, VARVARA G. ASOUTI AND KYRIAKOS C. GIANNAKOGLOU

Parallel CFD & Optimization Unit, School of Mechanical Engineering
National Technical University of Athens, Athens, Greece
e-mail: mkontou@mail.ntua.gr, xeftro@gmail.com, {vasouti,kgianna}@mail.ntua.gr

Key words: Adjoint, Discretization Schemes, Aerodynamic Shape Optimization, Transitional Flows

Summary. In aerodynamic shape optimization, gradient-based methods are regularly supported by the adjoint method computing the gradient of the objective function with respect to the design variables. The continuous adjoint offers a physical insight into the adjoint equations and low memory footprint; the accuracy of gradients is affected by the discretization schemes for the adjoint equations which are often decided by intuition, without necessarily being consistent with the primal ones. On the other hand, discrete adjoint computes sensitivity derivatives which are consistent with the discretized primal problem, with a higher memory footprint though. In this paper, the *Think-Discrete Do-Continuous* (*TDDC*) adjoint is extended to turbulent/transitional flows. The *TDDC* adjoint bridges the gap between the continuous and discrete adjoint by proposing consistent discretization schemes for the adjoint equations which are inspired by the hand-differentiated discrete adjoint, with a clear physical meaning though. The *TDDC* adjoint is verified on different grid sizes and used to solve shape optimization problems in turbulent/transitional external aerodynamics.

1 INTRODUCTION

In aerodynamic shape optimization (ShpO), gradient-based algorithms usually rely on the (continuous or discrete) adjoint method to compute the gradients of the objective function with respect to the design variables, since this is the most cost-effective way to do so. Working with continuous adjoint, [1, 2, 3], offers a clear physical insight into the adjoint equations (derived in the form of PDEs) and their boundary conditions and a low memory footprint of the adjoint code. Given that the adjoint equations must be discretized, finding appropriate discretization schemes is a challenge, since these can significantly affect the accuracy of the computed sensitivity derivatives (SDs). Their selection is based on intuition, by usually mimicking the primal discretization with some changes; for instance, an upwind primal scheme becomes downwind in the adjoint problem etc. This is not the case in discrete adjoint, [4, 5, 6], in which the adjoint equations result from the differentiation of the discretized primal problem, being fully consistent with the latter. Consequently, discrete adjoint has lack of understanding of the adjoint equations and, often, a high memory footprint.

Herein, discretization schemes for the continuous adjoint PDEs and their boundary conditions which are inspired by the discrete adjoint, and are, thus, consistent with the discretized primal problem are proposed. In specific, the advantages of continuous and discrete adjoint are combined into the *Think-Discrete Do-Continuous* (*TDDC*) adjoint. The *TDDC* adjoint computes SDs as accurate as discrete adjoint, by overcoming the usually high memory footprint of the latter; in addition, the *TDDC* adjoint retains the insight into the adjoint equations and boundary conditions. This work extends that of [7], which was dealing with the consistent discretization of the continuous adjoint to the Euler equations.

The *TDDC* discretization schemes are used for the ShpO of the NLF(1)-0416 (subsonic) and the RAE2822 (transonic) isolated airfoils in turbulent/transitional flow. For the latter, the Spalart–Allmaras turbulence model [8] is coupled with the $\gamma-\tilde{Re}_{\theta t}$ transition model, [9]. The proposed *TDDC* adjoint is developed using the in–house GPU-accelerated code PUMA, [10]. PUMA solves the Reynolds-Averaged Navier-Stokes (RANS) equations for compressible flows on unstructured/hybrid grids, using a vertex-centered finite volumes and second-order accuracy.

2 THE PRIMAL PROBLEM & ITS DISCRETIZATION

Dealing with compressible fluid flows which undergo transition, the so-called primal problem comprises the mean flow (MF) equations, the one-equation Spalart–Allmaras (SA) turbulence model, [8], the two-equation $\gamma-\tilde{Re}_{\theta t}$ transition model (the SA-sLM2015 variant of [9]) and the Hamilton-Jacobi equation computing distances Δ from the closest solid walls. In a 3D Cartesian coordinate system $x_k\,(k=1,2,3)$ the governing equations are

$$R_n^{\mathrm{MF}}=\frac{\partial f_{nk}^{\mathrm{inv}}}{\partial x_k}-\frac{\partial f_{nk}^{\mathrm{vis}}}{\partial x_k}=0\quad,\quad n=1,..,5 \tag{1a}$$

$$R^{\tilde{\nu}}=\frac{\partial\left(\rho v_k\tilde{\nu}\right)}{\partial x_k}-\frac{\rho}{\sigma}\left\{\frac{\partial}{\partial x_k}\left[\left(\nu+\tilde{\nu}\right)\frac{\partial\tilde{\nu}}{\partial x_k}\right]+c_{b_2}\frac{\partial\tilde{\nu}}{\partial x_k}\frac{\partial\tilde{\nu}}{\partial x_k}\right\}-\tilde{P}_{\tilde{\nu}}+\tilde{D}_{\tilde{\nu}}=0 \tag{1b}$$

$$R^{\gamma}=\frac{\partial\left(\rho v_k\gamma\right)}{\partial x_k}-\frac{\partial}{\partial x_k}\left[\left(\mu+\frac{\mu_t}{\sigma_f}\right)\frac{\partial\gamma}{\partial x_k}\right]-P_{\gamma}+E_{\gamma}=0 \tag{1c}$$

$$R^{\tilde{Re}_{\theta t}}=\frac{\partial\left(\rho v_k\tilde{Re}_{\theta t}\right)}{\partial x_k}-\frac{\partial}{\partial x_k}\left[\sigma_{\theta t}\left(\mu+\mu_t\right)\frac{\partial\tilde{Re}_{\theta t}}{\partial x_k}\right]-P_{\theta t}-D_{SCF}=0 \tag{1d}$$

$$R^{\Delta}=\frac{\partial}{\partial x_k}\left(\Delta\frac{\partial\Delta}{\partial x_k}\right)-\Delta\frac{\partial}{\partial x_k}\left(\frac{\partial\Delta}{\partial x_k}\right)-1=0 \tag{1e}$$

In 3D, Eqs. 1a are solved for the conservative flow variables $U_n=[\rho\ \ \rho v_1\ \ \rho v_2\ \ \rho v_3\ \ \rho E]^T$. The turbulent viscosity μ_t is given by $\mu_t=\rho\tilde{\nu}f_{v_1}$, where $\tilde{\nu}$ results from Eq. 1b. All undefined terms and constants in Eqs. 1b to 1d can be found in [8, 9]. Integrating Eqs. 1a-1e over a finite volume formed around node P and applying the Green-Gauss theorem results in a balance of fluxes; these are discretized on unstructured grids consisting of tetrahedra, pyramids, prisms and/or hexahedra. The finite volume Ω_P is shown in Fig. 1, in a 2D case, for demonstration purposes.

Below, the discretization of the primal fluxes is presented. All formulas refer to the finite volume Ω_P centered at node P with $\partial\Omega_P$ being its boundary. We refrain from providing expressions for the fluxes crossing the domain boundaries. The inviscid fluxes $\Phi_n^{\mathrm{inv},PQ}$ of Eqs. 1a,

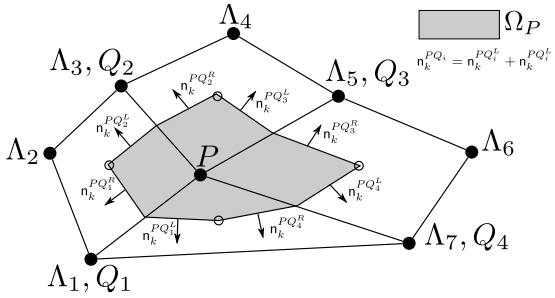

Figure 1: Vertex–centered finite volume formed around an internal node P. Normal vectors ($\mathbf{n}$) on the Ω_P boundaries have a magnitude equal to the area (or length in 2D) of the interface between two adjacent finite volumes. They point outwards and $\hat{\mathsf{n}}_k = \mathsf{n}_k/|\mathsf{n}|$. Nodes Q_i are connected to P via grid edges, $\mathcal{N}_e(P)=\{Q_i\}$, while nodes Λ_i are neighbors of P on the same grid element, $\mathcal{N}(P)=\{\Lambda_i\}$.

referring to $\frac{\partial f_{nk}^{\text{inv}}}{\partial x_k}$, are discretized using Roe's upwind scheme, [11], as

$$\Phi_n^{\text{inv},PQ} = \frac{1}{2}\left(A_{nmk}^P U_m^P + A_{nmk}^Q U_m^Q\right)\mathsf{n}_k^{PQ} - \frac{1}{2}\left|\tilde{A}_{nmk}^{LR}\mathsf{n}_k^{PQ}\right|\left(U_m^R - U_m^L\right) \tag{2}$$

where $A_{nmk} = \frac{\partial f_{nk}^{\text{inv}}}{\partial U_m}$ is the flux Jacobian, $f_{nk}^{\text{inv}} = A_{nmk}U_m$. $\left|\tilde{A}_{nmk}^{LR}\mathsf{n}_k\right|$ is the absolute Jacobian computed using the Roe–averaged quantities between the left (L) and right (R) states. Primitive flow variables V_m at L and R are extrapolated from P and Q as follows:

$$V_m^L = V_m^P + \frac{1}{2}\mathsf{t}_\ell^{PQ}\left.\frac{\partial V_m}{\partial x_\ell}\right|^P, \qquad \left.\frac{\partial V_m}{\partial x_\ell}\right|^P = D_\ell^P V_m^P + \sum_{\Lambda\in\mathcal{N}(P)} Z_\ell^{P\Lambda} V_m^\Lambda \tag{3a}$$

$$V_m^R = V_m^Q - \frac{1}{2}\mathsf{t}_\ell^{PQ}\left.\frac{\partial V_m}{\partial x_\ell}\right|^Q, \qquad \left.\frac{\partial V_m}{\partial x_\ell}\right|^Q = D_\ell^Q V_m^Q + \sum_{K\in\mathcal{N}(Q)} Z_\ell^{QK} V_m^K \tag{3b}$$

where D_ℓ, Z_ℓ are geometrical coefficients. $U_m^{L,R}$ are then computed from $V_m^{L,R}$. Fluxes $\Phi_{\text{conv}}^{\varphi,PQ}$ ($\varphi=\tilde{\nu},\gamma,\tilde{Re}_{\theta t}$), corresponding to convection terms in Eqs. 1b to 1d, are similarly discretized as

$$\Phi_{\text{conv}}^{\varphi,PQ} = \frac{1}{2}\left[(\rho v_k\varphi)^P + (\rho v_k\varphi)^Q\right]\mathsf{n}_k^{PQ} - \frac{1}{2}\left|(v_k\mathsf{n}_k)^{PQ}\right|\left[(\rho\varphi)^Q - (\rho\varphi)^P\right] \tag{4}$$

The viscous fluxes $\Phi_n^{\text{vis},PQ}$ in Eqs. 1a, corresponding to $\frac{\partial f_{nk}^{\text{vis}}}{\partial x_k}$, are $\Phi_{m+1}^{\text{vis},PQ} = \tau_{mk}^{PQ}\mathsf{n}_k^{PQ}, (m=1,2,3)$ and $\Phi_5^{\text{vis},PQ} = v_\ell^{PQ}\left(\tau_{\ell k}^{PQ} + q_k^{PQ}\right)\mathsf{n}_k^{PQ}$ with τ_{mk} and q_k being the stress tensor and the heat flux components, respectively. Computing τ_{mk}^{PQ}, q_k^{PQ} at the interface involves the spatial gradients of velocity and temperature (symbol ϕ) there, given by [12]

$$\left.\frac{\partial\phi}{\partial x_m}\right|_{PQ} = \left.\overline{\frac{\partial\phi}{\partial x_m}}\right|_{PQ} - \left[\left.\overline{\frac{\partial\phi}{\partial x_\ell}}\right|_{PQ}\hat{\mathsf{t}}_\ell - \frac{\phi^Q-\phi^P}{\sqrt{x_\ell^{PQ}x_\ell^{PQ}}}\right]\hat{\mathsf{t}}_m, \quad \left.\overline{\frac{\partial\phi}{\partial x_m}}\right|_{PQ} = \frac{1}{2}\left[\left.\frac{\partial\phi}{\partial x_m}\right|_P + \left.\frac{\partial\phi}{\partial x_m}\right|_Q\right], \quad \hat{\mathsf{t}}_m = \frac{x_m^Q - x_m^P}{\sqrt{x_\ell^{PQ}x_\ell^{PQ}}} \tag{5}$$

Eq. 5 is also used to discretize the diffusion terms in Eqs. 1b to 1d. Finally, any source term S_n^P (standing for $\tilde{P}_{\tilde{\nu}}$, $\tilde{D}_{\tilde{\nu}}$, P_γ, E_γ, $P_{\theta t}$ or D_{SCF}) at node P is assumed to be constant within Ω_P, thus $\int\limits_{\Omega_P} S_n \mathrm{d}\Omega \simeq S_n^P\Omega_P$.

3 THE *THINK-DISCRETE DO-CONTINUOUS* (*TDDC*) ADJOINT

For the objective function J, continuous adjoint starts by the augmented function $J_{\text{aug}} = J + \int_\Omega \left(\Psi_n R_n^{\text{MF}} + \tilde{\nu_a} R^{\tilde{\nu}} + \gamma_a R^{\gamma} + \tilde{Re}_a R^{\tilde{Re}_{\theta t}} + \Delta_a R^{\Delta} \right) \mathrm{d}\Omega$, where $\Psi_n, (n = 1, ..., 5)$ are the adjoint mean flow variables and $\tilde{\nu_a}$, γ_a, $\tilde{Re}_a$ and Δ_a are the adjoint to $\tilde{\nu}$, γ, $\tilde{Re}_{\theta t}$ and Δ, respectively. Differentiating J_{aug} w.r.t. the design variables b_i and setting the multipliers of $\frac{\delta \mathcal{U}_\ell}{\delta b_i}$ ($\mathcal{U}_\ell$, $\ell = 1, \ldots, 9$ with $\mathcal{U}_m := U_m$ for $m = 1, \ldots, 5$, $\mathcal{U}_6 := \rho\tilde{\nu}$, $\mathcal{U}_7 := \rho\gamma$, $\mathcal{U}_8 := \rho\tilde{Re}_{\theta t}$, $\mathcal{U}_9 := \Delta$) to zero leads to the field adjoint equations (FAE) and their boundary conditions, [13]. The FAE are written as

$$R_m^{\Psi} = -A_{nmk}\frac{\partial \Psi_n}{\partial x_k} - \mathcal{K}_m^{\text{MF}} + \mathcal{K}_m^{\text{SA}} + \mathcal{K}_m^{\gamma - \tilde{Re}_{\theta t}} = 0 \tag{6a}$$

$$R^{\tilde{\nu_a}} = -v_k\frac{\partial \tilde{\nu_a}}{\partial x_k} + \mathcal{G}^{\text{SA,diff}} + \mathcal{G}^{\text{SA,src}} + \mathcal{G}^{\mu_t,\text{MF}} + \mathcal{G}^{\mu_t,\gamma - \tilde{Re}_{\theta t}} = 0 \tag{6b}$$

$$R^{\gamma_a} = -v_k\frac{\partial \gamma_a}{\partial x_k} + \mathcal{H}^{\gamma - \tilde{Re}_{\theta t},\text{diff}} + \mathcal{H}^{\gamma - \tilde{Re}_{\theta t},\text{src}} + \mathcal{H}^{\text{SA,src}} = 0 \tag{6c}$$

$$R^{\tilde{Re}_a} = -v_k\frac{\partial \tilde{Re}_a}{\partial x_k} + \mathcal{N}^{\gamma - \tilde{Re}_{\theta t},\text{diff}} + \mathcal{N}^{\gamma - \tilde{Re}_{\theta t},\text{src}} + \mathcal{N}^{\text{SA,src}} = 0 \tag{6d}$$

$$R^{\Delta_a} = -2\frac{\partial}{\partial x_k}\left(\Delta_a\frac{\partial \Delta}{\partial x_k}\right) + \mathcal{M}^{\text{SA,src}} + \mathcal{M}^{\gamma - \tilde{Re}_{\theta t},\text{src}} = 0 \tag{6e}$$

$n = 1, \ldots, 5$, $m = 1, \ldots, 5$, $k = 1, \ldots, 3$. $\mathcal{K}_m^{\text{MF}} = \left(\frac{\partial \tau_{kq}^{\text{adj}}}{\partial x_k} - \tau_{kq}\frac{\partial \Psi_5}{\partial x_k}\right)\frac{\partial v_q}{\partial U_m} + \frac{\partial q_k^{\text{adj}}}{\partial x_k}\frac{\partial T}{\partial U_m}$, where τ_{km}^{adj} is the adjoint stress tensor $\tau_{mk}^{\text{adj}} = (\mu + \mu_t)\left[\frac{\partial \Psi_{m+1}}{\partial x_k} + \frac{\partial \Psi_{k+1}}{\partial x_m} + \frac{\partial \Psi_5}{\partial x_m}v_k + \frac{\partial \Psi_5}{\partial x_k}v_m - \frac{2}{3}\delta_{mk}\left(\frac{\partial \Psi_{\ell+1}}{\partial x_\ell} + \frac{\partial \Psi_5}{\partial x_\ell}v_\ell\right)\right]$ and q_k^{adj} the adjoint heat flux $q_k^{\text{adj}} = \mathcal{C}_p\left(\frac{\mu}{\text{Pr}} + \frac{\mu_t}{\text{Pr}_t}\right)\frac{\partial \Psi_5}{\partial x_k}$. The superscript in each term on the right-hand-side of Eqs. 6 denotes its origin. Their analytical expressions can be found in [13].

The proposed *TDDC* schemes exactly reproduce the outcome of the hand-differentiated discrete adjoint equations. Recall that, in discrete adjoint, J in discrete form is augmented by the inner product of the discretized residuals of the primal equations and the corresponding adjoint field variables, resulting in J_{aug}. Differentiating J_{aug} and eliminating the terms with derivatives of $\mathcal{U}_\ell$ w.r.t. b_i leads to the discrete adjoint equations. The *TDDC* adjoint also affects the discretization of the SDs; this is omitted in the interest of space.

3.1 *TDDC* Discretization of the Adjoint Mean Flow Equations

The integration of the inviscid term of Eq. 6a over Ω_P results in the balance of the corresponding adjoint fluxes (notations as in Fig. 1)

$$-\int_{\Omega_P} A_{nmk}\frac{\partial \Psi_n}{\partial x_k} d\Omega \simeq \sum_{Q \in \mathcal{N}_e(P)} \Phi_m^{\text{inv,adj},PQ} + \sum_{f \in \mathcal{B}(P)} \Phi_m^{\text{inv,adj},f} \tag{7}$$

With discrete adjoint guiding us, the *TDDC* discretization of internal fluxes yields

$$\Phi_m^{\text{inv,adj},PQ} = -\frac{1}{2}\left(\Psi_n^P + \Psi_n^Q\right) A_{nmk}^P \mathsf{n}_k^{PQ} - \frac{1}{2}\left[\left(\left|\tilde{\mathcal{A}}_{n\ell k}^{LR}\mathsf{n}_k\right|\Psi_n\right)^{R,\text{adj}} - \left(\left|\tilde{\mathcal{A}}_{n\ell k}^{LR}\mathsf{n}_k\right|\Psi_n\right)^{L,\text{adj}}\right]\frac{\partial V_\ell^P}{\partial U_m^P} \tag{8}$$

This is a non-conservative scheme, in contrast to the conservative one used in the primal problem, Eq. 2. In Eq. 8, for second–order accuracy, the "L"eft and "R"ight adjoint states are given by

$$\phi^{L,\mathrm{adj}} = \phi^P + \frac{1}{2}\left.\frac{\partial(\mathsf{t}_r\phi)}{\partial x_r}\right|^{P,\mathrm{adj}}, \left.\frac{\partial(\mathsf{t}_r\phi)}{\partial x_r}\right|^{P,\mathrm{adj}} = \mathsf{t}_r^{PQ} D_r^P \phi^P + \sum_{\Lambda\in\mathcal{N}(P)} Z_r^{\Lambda P} \sum_{M\in\mathcal{N}_e(\Lambda)} \mathsf{t}_r^{\Lambda M}\phi^\Lambda \tag{9a}$$

$$\phi^{R,\mathrm{adj}} = \phi^Q + \frac{1}{2}\left.\frac{\partial(\mathsf{t}_r\phi)}{\partial x_r}\right|^{Q,\mathrm{adj}}, \left.\frac{\partial(\mathsf{t}_r\phi)}{\partial x_r}\right|^{Q,\mathrm{adj}} = \mathsf{t}_r^{PQ} D_r^P \phi^Q + \sum_{\Lambda\in\mathcal{N}(P)} Z_r^{\Lambda P} \sum_{M\in\mathcal{N}_e(\Lambda)} \mathsf{t}_r^{\Lambda M}\phi^M \tag{9b}$$

and M is any node connected to $\Lambda\in\mathcal{N}(P)$ by an edge. Here, $\left|\tilde{\mathcal{A}}_{n\ell k}^{LR}\mathsf{n}_k\right|$ is the modified absolute Jacobian, [7], which includes the derivatives of $\left|\tilde{A}_{nmk}^{LR}\mathsf{n}_k\right|$ w.r.t. the primitive flow variables. Moreover, the L and R adjoint states are defined differently than in the primal problem. In the primal problem, the L state of any primal variable ϕ, along edge PQ, results from a Taylor expansion as the sum of ϕ^P and the inner product of the half of $\overrightarrow{PQ}$ and the spatial gradient of ϕ at P, Eq. 3. This gradient depends on ϕ values at P and neighbors Λ_i (Fig. 1). In Eq. 9, $\phi^{L,\mathrm{adj}}$ at edge PQ is the sum of the value of ϕ at P and half of the divergence of vector $\overrightarrow{PQ}$ scaled by ϕ. Contrasting these two formulas (primal and adjoint) is illustrative and helps the familiarization of the reader with the *TDDC* adjoint.

Integrating the viscous term of Eq. 6a over Ω_P yields

$$-\int_{\Omega_P}\mathcal{K}_m^{\mathrm{MF}}\mathrm{d}\Omega = -\int_{\Omega_P}\left[\left(\frac{\partial\tau_{kq}^{\mathrm{adj}}}{\partial x_k} - \tau_{kq}\frac{\partial\Psi_5}{\partial x_k}\right)\frac{\partial v_q}{\partial U_m} + \frac{\partial q_k^{\mathrm{adj}}}{\partial x_k}\frac{\partial T}{\partial U_m}\right]\mathrm{d}\Omega \simeq -\sum_{Q\in\mathcal{N}_e(P)}\Phi_m^{\mathrm{vis,adj},PQ} - \sum_{f\in\mathcal{B}(P)}\Phi_m^{\mathrm{vis,adj},f} \tag{10}$$

Any internal flux $\Phi_m^{\mathrm{vis,adj},PQ}$ in Eq. 10 splits into three terms, namely

$$-\sum_{Q\in\mathcal{N}_e(P)}\left(\Phi_{q,\tau_{km}}^{\mathrm{vis,adj},PQ}\left.\frac{\partial v_q}{\partial U_m}\right|^P - \Phi_{q,v_m}^{\mathrm{vis,adj},PQ}\left.\frac{\partial v_q}{\partial U_m}\right|^P + \Phi_{q_k}^{\mathrm{vis,adj},PQ}\left.\frac{\partial T}{\partial U_m}\right|^P\right)$$

where subscripts τ_{km}, v_m, q_k denote the fluxes origin. Based on discrete adjoint, the *TDDC* discretization schemes for the adjoint viscous fluxes are

$$\begin{aligned}\Phi_{q,\tau_{km}}^{\mathrm{vis,adj},PQ} = &\left[(\mu+\mu_t)\,\mathsf{n}_k\left(\frac{\partial\Psi_{q+1}}{\partial x_k} + \frac{\partial\Psi_5}{\partial x_k}v_q\right)\right]_{PQ}^{\mathrm{adj}} + \left[(\mu+\mu_t)\,\mathsf{n}_q\left(\frac{\partial\Psi_{k+1}}{\partial x_k} + \frac{\partial\Psi_5}{\partial x_k}v_k\right)\right]_{PQ}^{\mathrm{adj}} \\ &- \left[\frac{2}{3}\delta_{kq}\,(\mu+\mu_t)\,\mathsf{n}_\ell\left(\frac{\partial\Psi_{\ell+1}}{\partial x_k} + \frac{\partial\Psi_5}{\partial x_k}v_\ell\right)\right]_{PQ}^{\mathrm{adj}} \\ \Phi_{q,v_m}^{\mathrm{vis,adj},PQ} = &\frac{1}{2}\left(\Psi_5^Q - \Psi_5^P\right)\tau_{kq}^{PQ}\mathsf{n}_k^{PQ}, \quad \Phi_{q_k}^{\mathrm{vis,adj},PQ} = \left[\mathcal{C}_p\left(\frac{\mu}{\mathrm{Pr}} + \frac{\mu_t}{\mathrm{Pr_t}}\right)\mathsf{n}_k\frac{\partial\Psi_5}{\partial x_k}\right]_{PQ}^{\mathrm{adj}}\end{aligned} \tag{11}$$

where the "adjoint spatial gradient" ($\left[B\frac{\partial\varphi_a}{\partial x_m}\right]_{PQ}^{\mathrm{adj}}$) of an adjoint quantity φ_a, multiplied by a primal quantity B, at the interface between P and Q, is (δ_{km} is the Kronecker symbol)

$$\left[B\frac{\partial\varphi_a}{\partial x_m}\right]_{PQ}^{\mathrm{adj}} = \frac{1}{2}\left[\left[B\left(\delta_{m\ell} - \hat{\mathsf{t}}_\ell\hat{\mathsf{t}}_m\right)\frac{\partial\varphi_a}{\partial x_\ell}\right]^{P,\mathrm{adj}} - \left[B\left(\delta_{m\ell} - \hat{\mathsf{t}}_\ell\hat{\mathsf{t}}_m\right)\frac{\partial\varphi_a}{\partial x_\ell}\right]^{Q,\mathrm{adj}}\right] + B^{PQ}\frac{\varphi_a^Q - \varphi_a^P}{\sqrt{x_\ell^{PQ}x_\ell^{PQ}}}\hat{\mathsf{t}}_m^{PQ} \tag{12}$$

In a "standard" discretization scheme, Eq. 5 (adapted to the adjoint problem) could have been used instead of Eq. 12, for the discretization of the adjoint viscous fluxes. An additional difference between "standard" and *TDDC* adjoint is the edge which the primal quantity B is computed on. In the "standard" scheme, B is computed on edge PQ and is, then, multiplied by $\frac{\partial \varphi_a}{\partial x_m}\Big|_{PQ}$, as in Eq. 5. In the *TDDC* adjoint, B is not computed at PQ but at the edge appearing in the computation of the "adjoint spatial gradient", see Eqs. 9 and 12. Discretization schemes for the boundary fluxes can be found in [7].

The source terms of the adjoint mean flow equations, Eq. 6a ($\mathcal{K}_m^{\mathrm{SA}}$, $\mathcal{K}_m^{\gamma-\tilde{R}e_{\theta t}}$) arise from the differentiation of the SA and the $\gamma-\tilde{R}e_{\theta t}$ models. Those coming from the differentiation of the convection terms of the SA and $\gamma-\tilde{R}e_{\theta t}$ equations are written as

$$-\int_{\Omega_P}\rho\varphi\frac{\partial\varphi_a}{\partial x_k}\frac{\partial v_k}{\partial U_m}\mathrm{d}\Omega \simeq \sum_{Q\in\mathcal{N}_e(P)}\Phi_{k,\mathrm{conv}}^{\mathrm{src,adj},PQ}\frac{\partial v_k^P}{\partial U_m^P}+\sum_{f\in\mathcal{B}(P)}\Phi_{k,\mathrm{conv}}^{\mathrm{src,adj},f}\frac{\partial v_k^P}{\partial U_m^P}$$

$$\Phi_{k,\mathrm{conv}}^{\mathrm{src,adj},PQ}=-\frac{1}{2}\Big[(\rho\varphi)^P\big(\varphi_a^P+\varphi_a^Q\big)\mathsf{n}_k^{PQ}+\frac{1}{2}\big(\varphi_a^P-\varphi_a^Q\big)\Big((\rho\varphi)^Q-(\rho\varphi)^P\Big)sign\Big(v_k^{PQ}\mathsf{n}_k^{PQ}\Big)\mathsf{n}_k^{PQ}\Big] \tag{13}$$

and $\Phi_{k,\mathrm{conv}}^{\mathrm{src,adj},f}=0$, where φ and φ_a stand for $\tilde{\nu},\gamma,\tilde{R}e_{\theta t}$ and $\tilde{\nu_a},\gamma_a,\tilde{R}e_a$, respectively. Terms originating from the differentiation of the SA diffusion become

$$\sum_{\varphi=\rho,\nu,\tilde{\nu}}\left(\sum_{Q\in\mathcal{N}_e(P)}\Phi_{\mathrm{diff,SA},\varphi}^{\mathrm{src,adj},PQ}\frac{\partial\varphi^P}{\partial\rho^P}+\sum_{f\in\mathcal{B}(P)}\Phi_{\mathrm{diff,SA},\varphi}^{\mathrm{src,adj},f}\frac{\partial\varphi^P}{\partial\rho^P}\right)$$

$$\Phi_{\mathrm{diff,SA},\rho}^{\mathrm{src,adj},\alpha\beta}=-\frac{1}{\sigma}\tilde{\nu_a}^P\left[\nu^{\alpha\beta}+(1+c_{b_2})\,\tilde{\nu}^{\alpha\beta}-c_{b_2}\tilde{\nu}^P\right]\frac{\partial\tilde{\nu}}{\partial x_k}\Big|_{\alpha\beta}\mathsf{n}_k^{\alpha\beta},\quad \alpha\beta=PQ \text{ or } f \tag{14}$$

In *TDDC* adjoint, terms coming from the differentiation of the γ and $\tilde{R}e_{\theta t}$ diffusion become

$$-\int_{\Omega_P}\frac{\varphi}{\rho}\frac{\partial}{\partial x_k}\left[\sigma_{\varphi 1}\left(\mu+\frac{\mu_t}{\sigma_{\varphi 2}}\right)\frac{\partial\varphi_a}{\partial x_k}\right]\mathrm{d}\Omega \simeq -\sum_{Q\in\mathcal{N}_e(P)}\Phi_{\mathrm{diff},\varphi}^{src,\mathrm{adj},PQ}\frac{\varphi^P}{\rho^P}-\sum_{f\in\mathcal{B}(P)}\Phi_{\mathrm{diff},\varphi}^{src,\mathrm{adj},f}\frac{\varphi^P}{\rho^P}$$

$$\Phi_{\mathrm{diff},\varphi}^{src,\mathrm{adj},PQ}=\left[\sigma_{\varphi 1}\left(\mu+\frac{\mu_t}{\sigma_{\varphi 2}}\right)\mathsf{n}_k\frac{\partial\varphi_a}{\partial x_k}\right]_{PQ}^{\mathrm{adj}},\quad \Phi_{\mathrm{diff},\varphi}^{src,\mathrm{adj},f}=\frac{\partial}{\partial x_k}\left[\sigma_{\varphi 1}\left(\mu+\frac{\mu_t}{\sigma_{\varphi 2}}\right)\mathsf{n}_k\frac{\partial\varphi_a}{\partial x_k}\right]^{f,\mathrm{adj}} \tag{15}$$

For the discretization of the terms arising from the differentiation of the SA and γ–$\tilde{R}e_{\theta t}$ diffusion, Eqs. 9 and 12 are used for the boundary and internal fluxes, respectively. For the γ equation, $\sigma_{\varphi 1}$=1, $\sigma_{\varphi 2}$=σ_f, and for the $\tilde{R}e_{\theta t}$ equation $\sigma_{\varphi 1}$=$\sigma_{\theta t}$, $\sigma_{\varphi 2}$=1. The remaining terms come from the differentiation of the vorticity and strain rate magnitude, the velocity acceleration along the streamwise direction and the streamwise vorticity that are present in the SA and $\gamma-\tilde{R}e_{\theta t}$ sources, [8, 9], all of them containing the gradient of the velocity component. Based on the *TDDC* adjoint, these should be discretized using Eq. 9.

3.2 *TDDC* Discretization of the Adjoint Turbulence/Transition Models

Integrating the convection terms of Eqs. 6b, 6c and 6d over Ω_P, one gets ($\varphi_a = \tilde{\nu_a}, \gamma_a$ or $\tilde{Re}_a$)

$$
\begin{aligned}
-\int_{\Omega_P} v_k \frac{\partial \varphi_a}{\partial x_k} \mathrm{d}\Omega &\simeq \sum_{Q \in \mathcal{N}_e(P)} \Phi_{\mathrm{conv}}^{\varphi_a, PQ} + \sum_{f \in \mathcal{B}(P)} \Phi_{\mathrm{conv}}^{\varphi_a, f} \\
\Phi_{\mathrm{conv}}^{\varphi_a, PQ} = -\frac{1}{2}\left(\varphi_a^P + \varphi_a^Q\right) v_k^P \mathsf{n}_k^{PQ} - \frac{1}{2}\left(\varphi_a^Q - \varphi_a^P\right) \left| v_k^{PQ} \mathsf{n}_k^{PQ} \right|, \quad & \Phi_{\mathrm{conv}}^{\varphi_a, f} = 0
\end{aligned} \tag{16}
$$

As expected, the *TDDC* adjoint proposes the downwind discretization of the internal fluxes, in contrast to the upwind of the primal problem, and zero flux at all boundaries.

In Eq. 6b, the diffusion term is discretized as

$$
\begin{aligned}
-\int_{\Omega_P} \mathcal{G}^{\mathrm{SA},diff} \mathrm{d}\Omega &= \int_{\Omega_P} \frac{1}{\sigma} \left[(1+c_{b_2}) \frac{\partial (\rho \tilde{\nu_a})}{\partial x_k} \frac{\partial \tilde{\nu}}{\partial x_k} + c_{b_2} \rho \tilde{\nu_a} \frac{\partial}{\partial x_k} \left(\frac{\partial \tilde{\nu}}{\partial x_k} \right) \right] \frac{1}{\rho} \mathrm{d}\Omega \\
&\quad - \int_{\Omega_P} \frac{1}{\sigma} \left[\frac{\partial}{\partial x_k} \left[\left[\nu + (1+c_{b_2}) \tilde{\nu} \right] \frac{\partial (\rho \tilde{\nu_a})}{\partial x_k} \right] - c_{b_2} \frac{\partial}{\partial x_k} \left(\frac{\partial (\rho \tilde{\nu_a} \tilde{\nu})}{\partial x_k} \right) \right] \frac{1}{\rho} \mathrm{d}\Omega \\
&\simeq \sum_{Q \in \mathcal{N}_e(P)} \Phi_{\mathrm{diff}}^{\tilde{\nu_a}, PQ} \frac{1}{\rho^P} + \sum_{f \in \mathcal{B}(P)} \Phi_{\mathrm{diff}}^{\tilde{\nu_a}, f} \frac{1}{\rho^P}
\end{aligned}
$$

$$
\Phi_{\mathrm{diff}}^{\tilde{\nu_a}, PQ} = \frac{1}{\sigma} \left[(1+c_{b_2}) (\rho \tilde{\nu_a})^{PQ} - (\rho \tilde{\nu_a})^P \right] \left. \frac{\partial \tilde{\nu}}{\partial x_k} \right|_{PQ} \mathsf{n}_k^{PQ} - \frac{1}{\sigma} \left[\left[\nu + (1+c_{b_2}) \tilde{\nu} \right] \frac{\partial (\rho \tilde{\nu_a})}{\partial x_k} \mathsf{n}_k - c_{b_2} \frac{\partial (\rho \tilde{\nu_a} \tilde{\nu})}{\partial x_k} \mathsf{n}_k \right]_{PQ}^{\mathrm{adj}} \tag{17}
$$

$$
\Phi_{\mathrm{diff}}^{\tilde{\nu_a}, f} = -\frac{1}{\sigma} (\rho \tilde{\nu_a})^P \left. \frac{\partial \tilde{\nu}}{\partial x_k} \right|_f - \frac{1}{\sigma} \frac{\partial}{\partial x_k} \left[\left[(\rho \tilde{\nu_a}) \left[\nu + (1+c_{b_2}) \tilde{\nu} \right] - c_{b_2} (\rho \tilde{\nu_a} \tilde{\nu}) \right] \mathsf{n}_k \right]^{f,\mathrm{adj}} \tag{18}
$$

Regarding the adjoint transition model, integrating the diffusion terms of Eqs. 6c and 6d ($\mathcal{H}^{\gamma - \tilde{Re}_{\theta t}, diff}$ and $\mathcal{N}^{\gamma - \tilde{Re}_{\theta t}, diff}$) over Ω_P, leads to

$$
\begin{aligned}
-\int_{\Omega_P} \frac{1}{\rho} \frac{\partial}{\partial x_k} \left[\sigma_{\varphi 1} \left(\mu + \frac{\mu_t}{\sigma_{\varphi 2}} \right) \frac{\partial \varphi_a}{\partial x_k} \right] \mathrm{d}\Omega &\simeq - \sum_{Q \in \mathcal{N}_e(P)} \Phi_{\mathrm{diff}}^{\varphi_a, PQ} \frac{1}{\rho^P} - \sum_{f \in \mathcal{B}(P)} \Phi_{\mathrm{diff}}^{\varphi_a, f} \frac{1}{\rho^P} \\
\Phi_{\mathrm{diff}}^{\varphi_a, PQ} = \left[\sigma_{\varphi 1} \left(\mu + \frac{\mu_t}{\sigma_{\varphi 2}} \right) \mathsf{n}_k \frac{\partial \varphi_a}{\partial x_k} \right]_{PQ}^{\mathrm{adj}}, \quad & \Phi_{\mathrm{diff}}^{\varphi_a, f} = \frac{\partial}{\partial x_k} \left[\sigma_{\varphi 1} \left(\mu + \frac{\mu_t}{\sigma_{\varphi 2}} \right) \mathsf{n}_k \frac{\partial \varphi_a}{\partial x_k} \right]^{f,\mathrm{adj}}
\end{aligned} \tag{19}
$$

Following the discretization of the diffusion of the adjoint mean flow equations, in the *TDDC* adjoint, Eqs. 9 and 12 are proposed for the spatial gradients; in contrast, a "standard" discretization scheme would rely on Eqs. 3 and 5. For the source terms $\mathcal{G}^{\mu_t,\mathrm{MF}}$ and $\mathcal{G}^{\mu_t, \gamma - \tilde{Re}_{\theta t}}$

$$
\begin{aligned}
\int_{\Omega_P} \left[\mathcal{G}^{\mu_t,\mathrm{MF}} + \mathcal{G}^{\mu_t, \gamma - \tilde{Re}_{\theta t}} \right] \mathrm{d}\Omega &\simeq \sum_{Q \in \mathcal{N}_e(P)} \Phi_{\mathrm{adj},\mu_t}^{PQ} \frac{\partial \mu_t^P}{\partial \tilde{\mu}^P} + \sum_{f \in \mathcal{B}(P)} \Phi_{\mathrm{adj},\mu_t}^{f} \frac{\partial \mu_t^P}{\partial \tilde{\mu}^P} \\
&\quad + \sum_{Q \in \mathcal{N}_e(P)} \Phi_{\mathrm{adj},\mu_t}^{\gamma - \tilde{Re}_{\theta t}, PQ} \frac{\partial \mu_t^P}{\partial \tilde{\mu}^P} + \sum_{f \in \mathcal{B}(P)} \Phi_{\mu_t}^{\gamma - \tilde{Re}_{\theta t}, f} \frac{\partial \mu_t^P}{\partial \tilde{\mu}^P} + \left[\mathcal{C}_{\mathrm{adj},\mu_t}^{\gamma - \tilde{Re}_{\theta t}} \frac{\partial \mu_t}{\partial \tilde{\mu}} \right]^P \Omega_P
\end{aligned}
$$

$$
\begin{aligned}
\Phi^{PQ}_{\text{adj},\mu_t} &= \left[\left(\Psi^{PQ}_{m+1}-\Psi^{P}_{m+1}\right)+\left(\Psi^{PQ}_{5}-\Psi^{P}_{5}\right)v'^{PQ}_{m}\right]\mathsf{n}^{PQ}_{k}\frac{\tau^{PQ}_{km}}{\mu^{PQ}+\mu_t^{PQ}}+\mathcal{C}_p\left(\Psi^{PQ}_{5}-\Psi^{P}_{5}\right)\left.\frac{\partial T}{\partial x_k}\right|_{PQ}\mathsf{n}^{PQ}_{k} \\
\Phi^{f}_{\text{adj},\mu_t} &= -\left[\Psi^{P}_{m+1}+\Psi^{P}_{5}v'^{P}_{m}\right]\mathsf{n}^{f}_{k}\frac{\tau^{P}_{km}}{\mu^{P}+\mu_t^{P}}-\mathcal{C}_p\Psi^{P}_{5}\left.\frac{\partial T}{\partial x_k}\right|_{f}\mathsf{n}^{f}_{k} \\
\Phi^{\varphi_a,PQ}_{\text{adj},\mu_t} &= \left(\varphi^{PQ}_{a}-\varphi^{P}_{a}\right)\left.\frac{\partial \varphi}{\partial x_k}\right|_{PQ}\mathsf{n}^{PQ}_{k}\frac{\sigma_{\varphi 1}}{\sigma_{\varphi 2}}, \quad \Phi^{\varphi_a,f}_{\text{adj},\mu_t} = -\varphi^{P}_{a}\left.\frac{\partial \varphi}{\partial x_k}\right|_{f}\mathsf{n}^{f}_{k}\frac{\sigma_{\varphi 1}}{\sigma_{\varphi 2}}
\end{aligned}
\tag{20}
$$

where φ stands for the transition model variable $(\gamma, \tilde{Re}_{\theta t})$ and φ_a for its adjoint $(\gamma_a, \tilde{Re}_a)$.

The source terms in Eqs. 6b-6d are assumed to remain constant within Ω_P, yielding $\int\limits_{\Omega_P} S^{\text{adj}}_{\text{src}}\mathrm{d}\Omega \simeq S^{\text{adj},P}_{\text{src}}\Omega_P$, where $S^{\text{adj}}_{\text{src}}$ stands for $\mathcal{G}^{\text{SA},src}$, $\mathcal{H}^{\text{SA},src}$, $\mathcal{N}^{\text{SA},src}$, $\mathcal{H}^{\gamma-\tilde{Re}_{\theta t},src}$ and $\mathcal{N}^{\gamma-\tilde{Re}_{\theta t},src}$.

4 ShpO OF THE NLF(1)–0416 SUBSONIC AIRFOIL

The *TDDC* discretization schemes are firstly used in the ShpO of the NLF(1)-0416 isolated airfoil, [14], aiming at minimizing the drag coefficient (C_D), constrained by the lift coefficient (C_L) that should change no more than $\pm 1‰$ of the reference value. An additional constraint ensuring that the area of the airfoil does not drop below 90% of its reference one was also imposed. The flow conditions are $M_\infty = 0.1$, $Re = 4 \cdot 10^6$, turbulence intensity $T_u = 0.15\%$ and Angle of Attack AoA $= 2°$. At these flow conditions, the flow transitions from laminar to turbulent over both airfoil sides. The case is parameterized using the 8×7 volumetric NURBS (Non-Uniform Rational B-Splines) control grid, Fig. 2-left; the control points in blue remain constant while red ones are allowed to move in the normal-to-the-chord direction resulting in 12 design variables, in total.

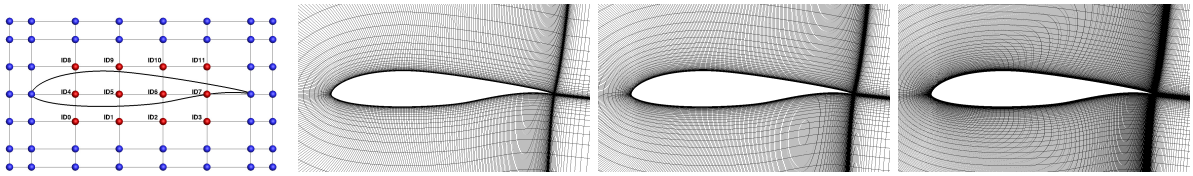

Figure 2: *NLF(1)–0416 Airfoil*: From left to right: Parameterization and grids of different quality, coarse 529×73, medium 705×97 and fine 1057×145 nodes.

The accuracy of the SDs computed using the "standard" and the *TDDC* adjoint on differently refined grids is investigated, Fig. 2. Reference SDs are computed using finite differences (FDs). The *TDDC* adjoint code reproduces the outcome of FDs with high accuracy on any grid, even the coarsest one, Fig. 3. In contrast, discrepancies appear on the SDs computed based on "standard" adjoint discretization; these are more intense in the C_D SDs and, in specific, for the design variables ID4 and ID8. After verifying the accuracy of the *TDDC* adjoint, the ShpO of the NLF(1)-0416 airfoil was performed on each grid, using the sequential least squares programming algorithm (SLSQP), [15]. The consistency of the proposed *TDDC* discretization schemes is beneficial for the ShpO, Fig. 4. On the coarse grid, the *TDDC* adjoint resulted in an optimized solution of better quality ($\sim$19%, instead of $\sim$15.1% reduction in C_D), in $\sim$37% less GPU cost, whereas a solution of same quality (i.e. about $\sim$21% reduction in C_D) was achieved in less cycles on the medium and fine grids.

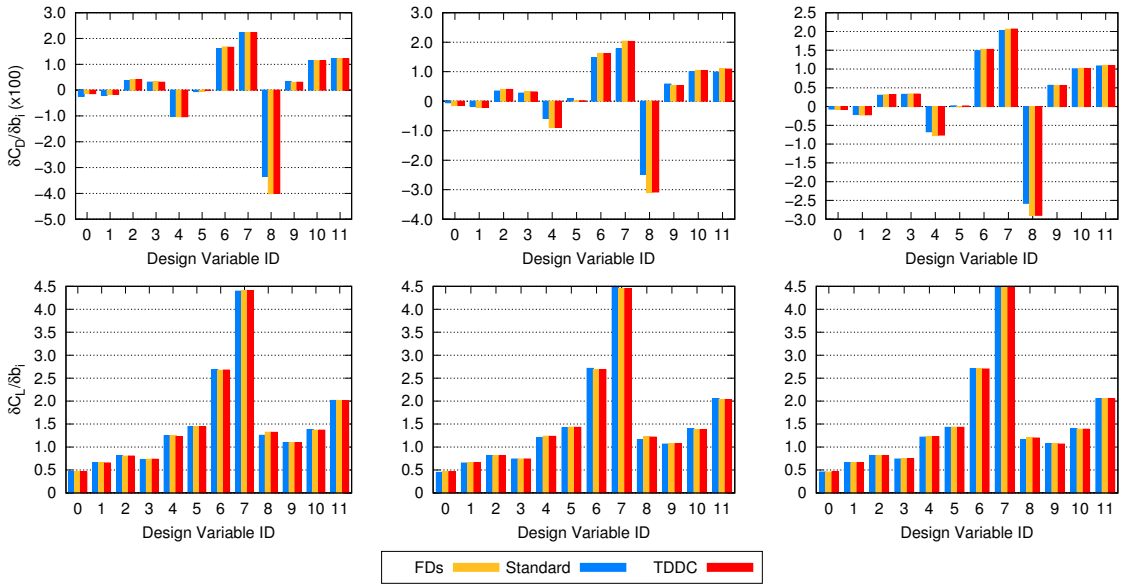

Figure 3: *NLF(1)–0416 Airfoil*: Comparison of C_D (top) and C_L (bottom) SDs computed by "standard" continuous (blue) and *TDDC* adjoint (red) as well as FDs (yellow). Coarse to fine grid from left to right.

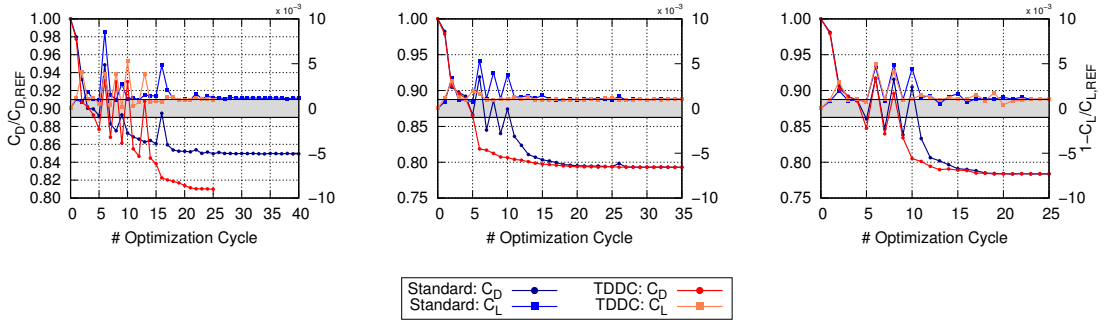

Figure 4: *NLF(1)–0416 Airfoil*: Evolution of C_D (objective) and C_L (constraint) during the ShpO for the coarse (left), medium (middle) and fine (right) grid based on the "standard" continuous (blue palette) and the *TDDC* (red palette) adjoint. The grayish area is associated with the C_L constraint and stands for the feasible zone. Each ShpO cycle includes one primal and two adjoint problem solutions.

The shape of the reference and the optimized airfoils based on the *TDDC* adjoint are presented in Fig. 5-left for all three grids. The ShpO resulted in similar airfoils with flattened pressure side and a suction side with increased curvature close to the trailing edge. The skin friction coefficient distribution for the reference and the optimized with the *TDDC* adjoint airfoils on the fine grid are shown in Fig. 5-right. The transition locations were shifted downstream both for the pressure and suction side, with a clear impact on C_D reduction.

5 ShpO OF THE RAE2822 TRANSONIC AIRFOIL

In the ShpO of the RAE2822 isolated airfoil at transonic flow conditions, the target and constraints are the same as in Sec. 4. The flow conditions are $M_\infty = 0.736$, $Re = 6.5 \cdot 10^6$ and

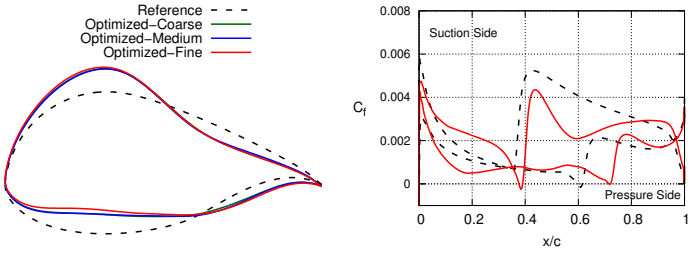

Figure 5: *NLF(1)–0416 Airfoil*: Shape (left; not in scale) and skin friction coefficient distribution (right) of the reference (black) and optimized (red) geometries, on the fine grid. The optimization used the *TDDC* adjoint.

AoA = 2.92°. Using a 10×7 NURBS control grid, Fig. 6, where the red control points are allowed to move in the normal-to-the-chord direction, the problem has 16 design variables.

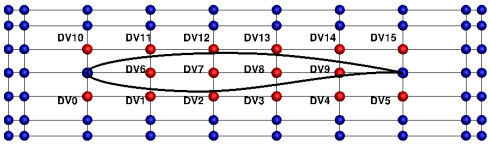

Figure 6: *RAE2822 Airfoil*: Parameterization.

Two ShpO studies were performed; the first was based on the SA turbulence model only (no transition model), while the second on the SA-sLM2015 transition model. For the latter, a low value of turbulence intensity was imposed at the far-field, $T_u = 0.05\%$. The accuracy of the SDs of C_D, C_L and the ShpO convergence histories are shown in Fig. 7. The *TDDC* adjoint computes accurate SDs with both flow models, even if, for the "standard" continuous adjoint, small discrepancies in the SDs can be seen. This is also reflected on the ShpO convergence. For the ShpO based on the SA model, the *TDDC* adjoint reached a solution of same quality (∼33.1% drop in C_D) in less cycles ensuring a "smoother" convergence of the imposed constraints. In the ShpO with the transition model, for the same number of cycles, the *TDDC* adjoint converged to a better solution than with the "standard" discretization schemes (∼45.9% instead of ∼41.6%). The Mach number fields for the reference and the optimized airfoils, based on the *TDDC* adjoint, are presented in Fig. 8. The strength of the shock wave was reduced in both optimizations and this led to lower C_D. Regarding the ShpO without the transition model, the airfoil became thinner close to the leading edge, while the use of the transition model increased the curvature of the suction side and shifted the highly curved part towards the trailing edge.

6 CONCLUSIONS

Consistent, with the primal problem, discretization schemes for the continuous adjoint PDEs, with a clear physical insight and low memory requirements of the adjoint code were developed. These were inspired by the hand–differentiated discrete adjoint equations which were firstly derived. The proposed *Think-Discrete Do-Continuous* (*TDDC*) adjoint was developed for the RANS equations, coupled with the Spalart–Allmaras turbulence model and the γ–$\tilde{Re}_{\theta t}$ transition model. Following the methodology of the *TDDC* adjoint, it was possible, for instance, to propose operators for the consistent discretization of adjoint terms that include the gradient of an adjoint quantity at any node P or any edge PQ, see Eqs. 9 and 12 to be used instead of Eqs. 3 and Eq. 5 of a "standard" approach. In fact, the development of the *TDDC* adjoint is the only way to come up with the aforementioned consistent discretization. The accuracy of

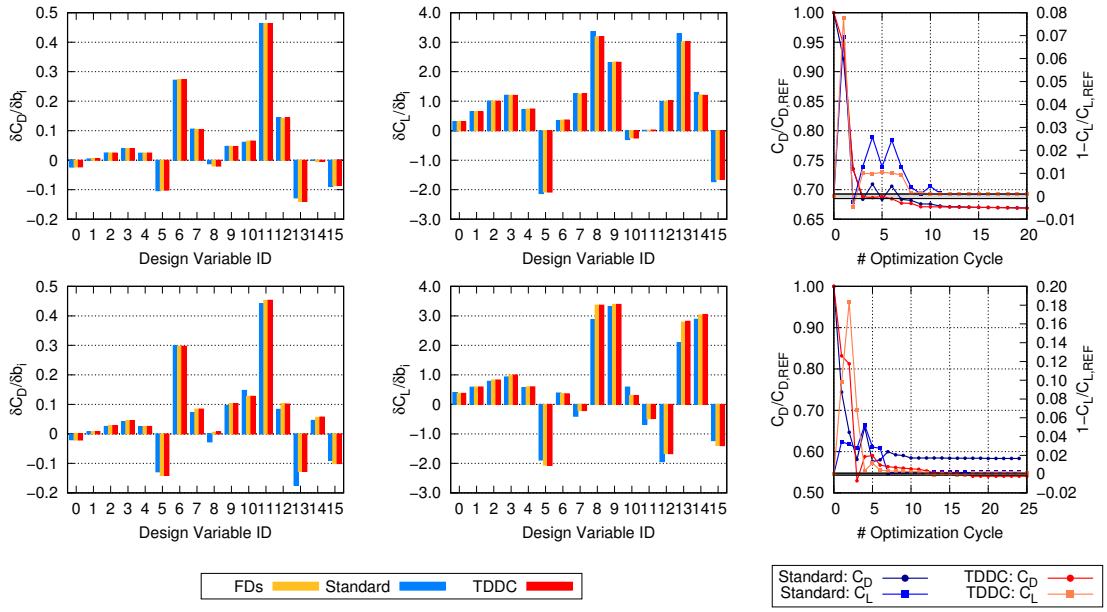

Figure 7: *RAE2822 Airfoil*: Comparison of C_D (left) and C_L (middle) SDs computed by the "standard" continuous (blue) and *TDDC* adjoint (red) as well as FDs (yellow). ShpO convergences (right) based on the two adjoint methods. Computations without (top) and with (bottom) the transition model.

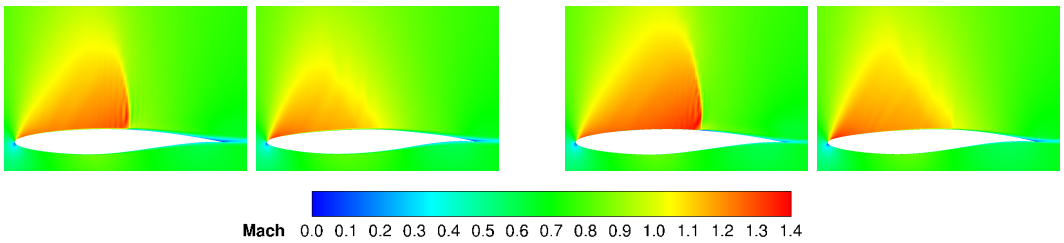

Figure 8: *RAE2822 Airfoil*: Mach number field for the reference (left) and the optimized airfoils (right). Computations without (first two) and with (last two) transition model.

the SDs of the *TDDC* adjoint, and its impact on the ShpO convergence, were demonstrated in the ShpO of two isolated airfoils in turbulent/transitional flow. Comparisons with "standard" adjoint discretization schemes, widely used in the literature, revealed the high accuracy of the *TDDC* adjoint in computing SDs and, consequently, the improved ShpO behavior (in terms of convergence and quality of the optimized solution). The proposed *TDDC* discretization schemes were also applied in an industrial application presented in a companion ECCOMAS 2024 paper (Kontou et al., *Continuous Adjoint-Based Optimization of a High Aspect-Ratio Wing Business Jet in Transitional Flows*).

7 ACKNOWLEDGMENT

This work was supported by the Hellenic Foundation for Research and Innovation (H.F.R.I.) under the "2nd Call for H.F.R.I. Research Projects to support Faculty Members & Researcher" (Project Number: 3821).

REFERENCES

[1] A. Jameson. Aerodynamic design via control theory. *J. Sci. Comput.*, 3, 1988.

[2] W. Anderson and V. Venkatakrishnan. Aerodynamic design optimization on unstructured grids with a continuous adjoint formulation. *Comput. Fluids*, 28(4):443 – 480, 1999.

[3] E. Papoutsis-Kiachagias, A. Zymaris, I. Kavvadias, D. Papadimitriou, and K. Giannakoglou. The continuous adjoint approach to the k–ε turbulence model for shape optimization and optimal active control of turbulent flows. *Eng. Optim.*, 47(3):370–389, 2015.

[4] J. Elliott and J. Peraire. Practical three-dimensional aerodynamic design and optimization using unstructured meshes. *AIAA J.*, 35(9):1479–1485, 1997.

[5] E. Nielsen and W. Anderson. Aerodynamic design optimization on unstructured meshes using the Navier-Stokes equations. *AIAA J.*, 37(11):1411–1419, 1999.

[6] M. Giles, M. Duta, and J. Muller. Adjoint code developments using the exact discrete approach. *15th AIAA Computational Fluid Dynamics Conference*, 2001.

[7] M. Kontou, X. Trompoukis, V. Asouti, and K. Giannakoglou. On the discretization of the continuous adjoint to the Euler equations in shape optimization. In *ADMOS 2023, International Conference on Adaptive Modeling and Simulation*, Gothenburg, Sweden, 2023.

[8] P. Spalart and S. Allmaras. A one-equation turbulence model for aerodynamic flows. *AIAA J.*, 439:5–21, 1992.

[9] M. Piotrowski and D. Zingg. Smooth local correlation-based transition model for the Spalart-Allmaras turbulence model. *AIAA J.*, 59:474–492, 2021.

[10] V. Asouti, X. Trompoukis, I. Kampolis, and K. Giannakoglou. Unsteady CFD computations using vertex-centered finite volumes for unstructured grids on Graphics Processing Units. *Int. J. Numer. Methods Fluids*, 67:232–246, 2011.

[11] P. Roe. Approximate Riemann solvers, parameter vectors, and difference schemes. *J. Comput. Phys.*, 43(2):357 – 372, 1981.

[12] J. Weiss, J. Maruszewski, and W. Smith. Implicit solution of preconditioned Navier-Stokes equations using algebraic multigrid. *AIAA J.*, 37(1):29–36, 1999.

[13] M. Kontou, X. Trompoukis, V. Asouti, and K. Giannakoglou. The continuous adjoint method to the $\gamma-\tilde{Re}_{\theta t}$ transition model coupled with the Spalart-Allmaras model for compressible flows. *Int. J. Numer. Methods Fluids*, https://doi.org/10.1002/fld.5319.

[14] D. Somers. Design and Experimental Results for a Natural-Laminar-Flow Airfoil for General Aviation Applications. *NASA Technical Paper 1861*, 1981.

[15] J. Nocedal and S. Wright. *Numerical Optimization.* Springer, 1999.